Geometrical optimization of rectangular MVGs delaying boundary layer transition over a flat plate

Márton KULCSÁR[1], András SZABÓ[2], Péter Tamás NAGY[2], György PAÁL[2]

[1] Corresponding Author. Department of Fluid Mechanics, Faculty of Mechanical Engineering, Budapest University of Technology and Economics. H-1111, Budapest, Műegyetem rkp. 3., D building, 3rd floor. E-mail: mkulcsar@hds.bme.hu
[2] Department of Hydrodynamic Systems, Faculty of Mechanical Engineering, Budapest University of Technology and Economics.

ABSTRACT

It has been shown both numerically [1] and experimentally [2] that employing miniature vortex generators (MVGs) to create spanwise mean velocity gradients (SVGs), which in turn attenuate the growth of Tollmien–Schlichting (TS) waves, can delay the transition from laminar to turbulent flow in a low-turbulence boundary layer over a flat plate.

Recently, a parametric study was carried out by Szabó et al. [3] which showed that the measurements carried out by Sattarzadeh et al. [4] utilised non-optimal vortex generators. Consequently, my aim was to find the optimal geometric parameters of MVGs for a given far-field velocity and streamwise position.

Finally, a Bayesian approach, following Ament et al. [5], is used to optimise the geometric properties of the MVGs.

Keywords: boundary layer, CFD, flow stability, MVG, optimization, transition delay

1. INTRODUCTION

Delaying laminar-turbulent transition is crucial for reducing friction drag on streamlined bodies. Transition occurs via boundary layer instabilities (natural transition) or bypass transition, determined by free-stream turbulence levels [6]. Bypass transition, prevalent at high turbulence, is complex and less suitable for control. Natural transition, occurring at low turbulence, is better understood, driven by the exponential growth of small disturbances like Tollmien-Schlichting (TS) waves, describable by linear stability theory, followed by a non-linear secondary instability phase [7]. Dampening TS waves is thus a key strategy for transition delay.

Various active (e.g., wall movement, suction) and passive (e.g., shape optimisation, localised surface modifications [8, 9]) techniques aim to delay transition. While structures like riblets can inhibit Görtler instabilities, they do not suppress TS waves [10, 11]. An effective TS wave dampening method involves introducing streamwise streaks (alternating slow/fast flow regions) into the boundary layer [12, 13]. These streaks induce spanwise shear, disrupting disturbance energy growth, a principle used in spanwise mean velocity gradient (SVG) methods [12, 14].

Generating boundary layer streaks is effective for flow stabilisation [15]. Higher amplitude streaks offer better stabilisation [12], but excessive amplitudes can trigger secondary sinuous instabilities and premature transition [16]. Passive methods are preferred over active ones due to no external energy requirement. Early passive attempts with cylindrical roughness elements had limited success, as increased height destabilised their wakes [13].

A promising passive approach involves winglet-type miniature vortex generators (MVGs), which create strong, stable streaks for effective boundary layer stabilisation [17]. Extensive experimental studies [18, 19, 20, 2, 21] explored MVG parameter influences, streak reinforcement, instability development, and pressure gradient effects, confirming TS wave [2] and oblique disturbance [22] stabilisation. Most studies utilised triangular MVGs, with some investigating rectangular designs [2, 4]. These findings established MVGs' efficacy in creating streaky boundary layers that attenuate TS wave growth. Recently, [23] applied MVGs to an aircraft fuselage, developing practical parameter selection guidelines.

Numerical investigations have further explored MVG flow stability. Siconolfi et al. [1] used Bi-Global stability analysis, finding reasonable agreement with experiments [19] but noted challenges in comparing disturbance growth near MVGs due to instability scattering. Nobis et al. [24] optimised MVG design using a direct-adjoint looping approach to minimise downstream TS wave energy, significantly improving performance but neglecting spanwise spacing, a key parameter for streak evolution [4, 25]. Most recently, Szabó et al. [3]conducted a

parametric study of 225 rectangular MVG configurations using steady-state simulations, Boundary Region Equations (BRE) for flow extension, and BiGlobal stability analysis. They varied MVG height, inter-pair, and intra-pair distances, finding that taller, more sparsely placed MVGs sustain stronger streaks.

Bayesian optimisation [26] is a technique for optimising expensive-to-evaluate functions, with applications in areas like fluid dynamics [27]. First, a probabilistic surrogate model (typically a Gaussian Process, GP) of the objective function is initialised and built using available data points. Then, an acquisition function determines the next sampling point by balancing exploration and exploitation. Finally, the objective function is evaluated at the new point(s), and the model is updated. The process iterates until a stopping criterion is met.

1.1. Objectives of the study

In this study, the stability of the streaky boundary layer generated by MVGs mounted on a zero-pressure-gradient flat plate is analysed using local modal linear stability analysis. As such, it is important to emphasise that the present study focuses specifically on using MVGs to delay the growth of TS waves. Therefore, the recommendations provided here may not necessarily yield improvements in all aspects of MVG design.

Unlike Pederson et al. [28] and Klauss et al. [29], who used streak amplitude as an indirect measure of boundary layer stabilisation, this study directly characterises the flow by solving local stability equations within the framework of the e^N method. Two N factors are computed, one for TS waves and another for secondary instabilities. While using two N factors to assess flow stability may seem unconventional, it is not unprecedented: Scrauf [30] successfully employed this approach by separately evaluating stationary crossflow instability and TS waves to correlate local stability calculations with in-flight test data.

Although the e^N method may appear simplistic compared to more recently developed stability analysis tools, it remains widely used in industrial applications [31, 32] due to its simplicity, relatively low computational cost, and ability to capture key aspects of the transition process. Its continued success suggests that it can provide valuable predictions.

This study focuses on rectangular MVGs, allowing the investigation of key parameters such as spanwise spacing, an aspect not considered in previous topology optimisation studies [28, 29, 24].

A Bayesian optimisation was conducted where three parameters were varied simultaneously: the height (h), the distance between MVGs in each pair (Λ), and the angle of the MVGs (θ). The aim of this optimisation, consistent with [28] and [29], was to attenuate primary instabilities while avoiding the emergence of secondary instability modes. The results can be found in Section 3.

2. FLOW CONFIGURATION AND MODELLING

2.1. Flow configuration

A zero-pressure-gradient incompressible boundary layer is considered. Dimensional quantities are denoted with a hat ($\hat{\square}$), while non-dimensional quantities are represented without it. The free-stream velocity is set to $\hat{U}_\infty = 6$ m/s, and the kinematic viscosity is $\hat{\nu} = 1.4607 \times 10^{-5}$ m^2/s. The problem setup is illustrated in Figure 1. The downstream distance from the idealised leading edge to the MVG centre is denoted as $\hat{x}_{\mathrm{MVG}}$. The spanwise distance between two MVGs is $\hat{d}$, and the spanwise distance between MVG pairs is $\hat{\Lambda}$. The MVGs have a width $\hat{w}$, length $\hat{L}$, and height $\hat{h}$, and are oriented at an angle $\hat{\theta}$ relative to the free-stream velocity. Recently, [3] found that an important metric for the distance between MVGs is its ratio to the distance between different pairs, as such, this ratio ($\hat{d}/\hat{\Lambda}$) was kept at a fixed value. The specific constant parameter values are provided in Table 1, along with their ratios to the boundary layer thickness at the MVG location ($\hat{\delta}_{99,\mathrm{MVG}} = 3.610$ mm). The parameters varied during the optimisation and their bounds are provided in Table 2, along with the same ratio as before.

2.2. Modelling

The stability of an incompressible boundary layer over a flat plate is analysed using linear stability theory. For a detailed description of the employed method, the reader is referred to [3]. In summary, the governing equations are non-dimensionalised with the free-stream velocity $\hat{U}_\infty$ and boundary layer length scale $\hat{\delta}_0 = \sqrt{\hat{L}_0 \hat{\nu}/\hat{U}_\infty}$. The length scale is $\hat{L}_0 = \hat{x}_{st}$ where $\hat{x}_{st}$ is the start of the BRE calculation, shown on Fig. 1. Because of these, the Reynolds number used in this paper is defined as $\mathrm{Re}_\delta = \hat{\delta}_0 \hat{U}_\infty/\hat{\nu}$. The velocity field is decomposed into a steady base flow and small perturbations. The base flow is calculated in two steps. First, near the MVGs, the complete NS equations are solved. Further downstream, they can be simplified under appropriate scaling assumptions. Introducing the small parameter ε, the boundary region equations (BRE) are derived, which extend the boundary layer equations and allow the efficient extension of the base flow downstream during the second step.

The stability of the streaky boundary layer is analysed using the BiGlobal stability framework [33]. Since the base flow varies weakly in the streamwise direction, disturbances are assumed to take the form of modal waves with a prescribed real frequency, while the complex wavenumber is computed as an eigenvalue. This leads to the BiGlobal stability equations, widely used in flow stability studies. The spatial growth rate is given by the imaginary part of the wavenumber, and the eigenvalue problem is solved using standard numerical methods. Finally, the growth rates from each slice are used to calculate
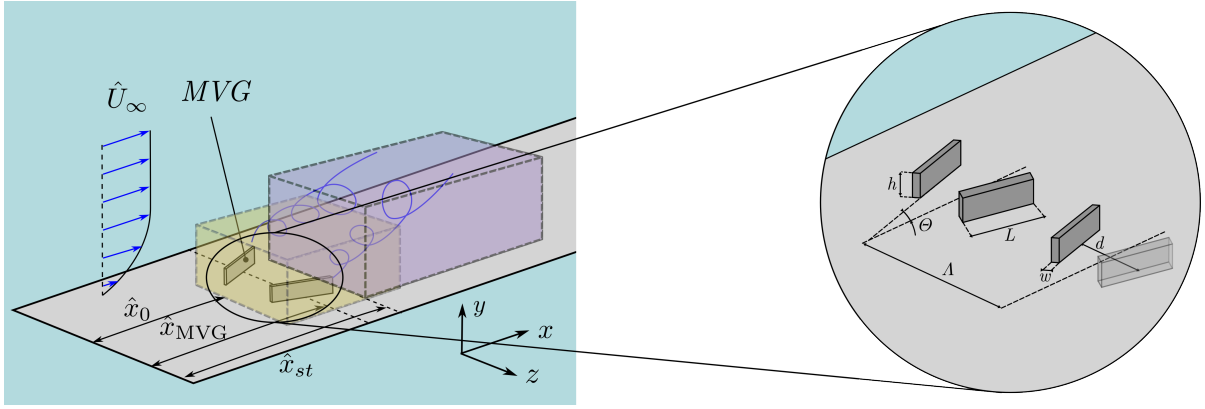
2

Figure 1. Flow configuration

Table 1. Constant parameters of the computational setup

$\hat{d}/\hat{\Lambda}$ $(-)$	$\hat{w}$ (mm)	$\hat{L}$ (mm)	$\hat{x}_{\mathrm{MVG}}$ (mm)	$\hat{x}_0$ (mm)	$\hat{x}_{\mathrm{st}}$ (mm)	$\hat{x}_{1,\mathrm{CFD}}$ (mm)
0.5	0.3	3.25	222	213	235	240
	$(0.083\delta_{99,\mathrm{MVG}})$	$(0.90\delta_{99,\mathrm{MVG}})$				

Table 2. Varied parameters of the computational setup

$\hat{\Lambda}$ (mm)	$\hat{h}$ (mm)	Θ (°)
[15, 100]	[0.9, 2.5]	[3, 15]
$[4.15, 27.70]\,\delta_{99,\mathrm{MVG}}$	$[0.25, 0.69]\,\delta_{99,\mathrm{MVG}}$	

the N factor to be used in the e^N method.

The transition to turbulence is predicted using the e^N method, where the transition location correlates with the growth of instability waves. The N factor is computed for each eigenmode, with transition occurring when a critical N value is reached. Two types of instabilities are considered: modified TS waves and secondary instabilities. TS waves, the primary instability in two-dimensional boundary layers, are weakened by streaks and dominate at low frequencies. In contrast, secondary instabilities arise due to streaks and exhibit a broader frequency range, often accelerating transition.

For TS waves, a conservative transition threshold of $N = 7$ is used. No established threshold exists for secondary instabilities, so the maximum N value among all unstable modes is tracked.

2.3. Numerical solution and parameters

The base flow computation consists of two steps: first, the near-MVG flow is computed using 3D CFD, followed by solving the BRE for the downstream flow. BRE calculations start slightly upstream of the CFD domain's end to prevent any effects from the boundary condition.

The CFD simulation employs ANSYS CFX 21 R2 [34], using a steady-state solver. To reduce the computational cost, only half of the geometry (a single MVG) was simulated, while the rest of the computational domain was accounted for by prescribing symmetry boundary conditions to the base flow. A Blasius profile is imposed upstream, while a free-outflow boundary is applied downstream to al-

low backflow into the domain. The mesh is generated with GMSH [35]. As shown in the figure, the mesh is finest near the MVG, with element size progressively increasing further away. A typical mesh contains approximately $8 - 16 \cdot 10^6$ elements. Second-order spatial discretisation is used, and mesh refinement tests confirm negligible sensitivity in results.

The BRE and BiGlobal stability equations are solved using a finite element method, implemented in the parallel version of the open-source finite element library FreeFem [36]. Taylor-Hood elements are used, where the velocity and pressure fields are discretised using $\mathcal{P}_2$ and $\mathcal{P}_1$ elements, respectively. The mesh, consisting of triangular elements, is generated using BAMG [37], the built-in mesh generator of FreeFem, which utilises Delaunay triangulation to discretise the domain. It adapts element sizes for efficient wall-normal and spanwise resolution. Further mesh refinement studies verified that increased resolution has minimal effect on transition Reynolds numbers.

BRE equations are discretised with a second-order backward Euler scheme, using PETSc [38] for sparse linear algebra and SLEPc [39] for eigenvalue computations. The non-linear system of equations arising from the discretisation of the BRE is solved using a second-order line search (Newton-Raphson) method with the SNES library of PETSc. LU factorisation via MUMPS [40] ensures efficient Jacobian inversion.

BiGlobal stability calculations employ the Krylov-Schur algorithm with shift-invert techniques. This approach enables the extraction of eigenvalues

3

near an initial guess, referred to as the shift. For each MVG configuration, streamwise location, and frequency, multiple eigenvalue calculations with varying shifts are performed to capture the relevant portion of the spectrum. Shifts are adjusted dynamically to ensure unstable modes are reliably tracked downstream. If an eigenvalue is lost, an additional shift is introduced based on the most unstable mode, guaranteeing accurate instability detection.

Two sets of stability analyses are conducted: one for the modified TS waves and another for the secondary instabilities.

2.4. Optimisation

In order to efficiently explore the parameter space and identify optimal configurations, a multi-objective Bayesian optimisation approach was implemented using the BoTorch [41] package for Python. The logNEHVI (log-constrained Noisy Expected Hypervolume Improvement) [5] acquisition function was employed to maximise two competing objectives. The first of these is the transitional Reynolds number in the low-frequency TS wave domain, which should be maximised. The second is the maximum growth rate of secondary instabilities, which should be minimised, but was multiplied by -1 to reformulate it as a maximisation problem. We assume that our results are exact, so the acquisition function was used in a noiseless setting, this increases numerical stability compared to using the logEHVI (log-constrained Expected Hypervolume Improvement) formulation. The parameter space was constrained using the non-linear constraint handling capabilities of BoTorch to ensure physically relevant configurations. These constraints ensured that two MVGs in the same pair can not touch:

$$\hat{d} - 2 \cdot \hat{L} \cdot sin(\Theta) > \frac{\hat{w}}{2} \tag{1}$$

and that two MVGs in different pairs could not touch:

$$\hat{d} + 2 \cdot \hat{L} \cdot sin(\Theta) < \hat{\Lambda} - \frac{\hat{w}}{2} \tag{2}$$

To accelerate convergence, four new points were queried and evaluated in each iteration step. The goal was to identify a Pareto frontier, balancing both objectives, and the optimisation process was terminated once a sufficient number of Pareto-optimal points were found.

During the optimisation three parameters were varied to validate the viability of the optimisation process, so that it can be used in the future for broader sets of parameters. The constant parameters, such as the streamwise velocity, streamwise position of the MVGs, etc. are shown in Table 1. The bounds of the varied parameters are shown in Table 2. In this three-parameter run, relevant results from the aforementioned parameter study [3] were used as initial

data to guide the optimization. This approach facilitated an accelerated convergence toward the Pareto-optimal solutions.

3. RESULTS

In this section, the results obtained from the previously outlined modelling framework are presented. A total of 87 points were evaluated in the model, with 28 taken from the initial parameter study [3] and 59 newly queried points. As demonstrated by the Pareto frontier, Fig. 2a, previous results from [3] and [4] were significantly improved. The best-performing configuration reached the end of the computational domain without triggering the laminar-turbulent transition while maintaining low amplification of secondary instabilities. The convex hull highlights theoretically ideal points, which slightly outperform some of the Pareto-optimal configurations, suggesting that further evaluations could lead to Pareto-optimal points aligning more closely with these theoretically ideal ones. All newly tested points are shown in Fig. 2b, with MVG height and spacing scaled by factors of 10^4 and 10^3, respectively, to emphasise trends rather than absolute values. Full markers indicate Pareto-optimal points, while opaque ones represent suboptimal configurations. The x-axis denotes the transition Reynolds number. The figure reveals distinct optimal ranges for both MVG angle and spacing, while height remains maximised in all optimal cases. The angle effect can be attributed to the need for a sufficiently strong vortex to generate a streaky boundary layer without excessively amplifying secondary instabilities. The optimum MVG spacing arises from the necessity of streak interactions, if too close, they break down prematurely; if too far apart, they fail to sustain each other. The consistently maximal height suggests that vortices generated higher in the boundary layer have a stronger influence on TS wave modulation. However, the upper bound was not extended further, as excessively tall MVGs might trigger transition mechanisms beyond the capabilities of the model.

Two points from the Pareto-frontier, the ones with the highest transitional Reynolds-numbers were further analysed, the parameters of these configurations, along with the best points from [3] and [4] are summarized in Table 3

The amount of drag reduction achieved can be quantified using an averaged drag coefficient (c_D) which is calculated in the following way:

$$c_D = \frac{\frac{\hat{F}_{MVG}}{\hat{U}_\infty^2 \cdot \hat{\rho} \cdot \hat{\Lambda}/2} + \int_{\hat{x}_{st}}^{\hat{x}_1} c_f(\hat{x}) \, d\hat{x}}{\hat{x}_1 - \hat{x}_0} \tag{3}$$

Where c_f is the skin friction coefficient which can be seen in Fig. 3 and F_{MVG} is queried from the laminar CFD of the first phase of the calculation. The figure is shown as a function of Re_δ to be consistent with the other figures. For the turbulent part of the function the Schultz-Grunow formula [42] was used.

4
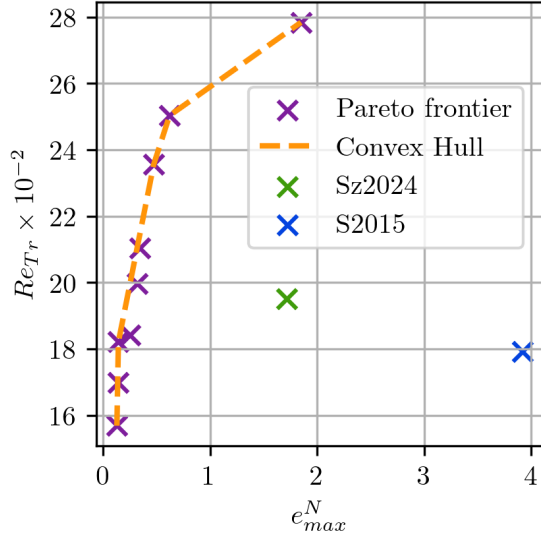
(a) Pareto frontier; the x-axis is the maximum N factor calculated for the secondary instabilities, while the y-axis show the transition Reynolds number. The points from [3] and [4] are the best points from their studies according to our criteria.
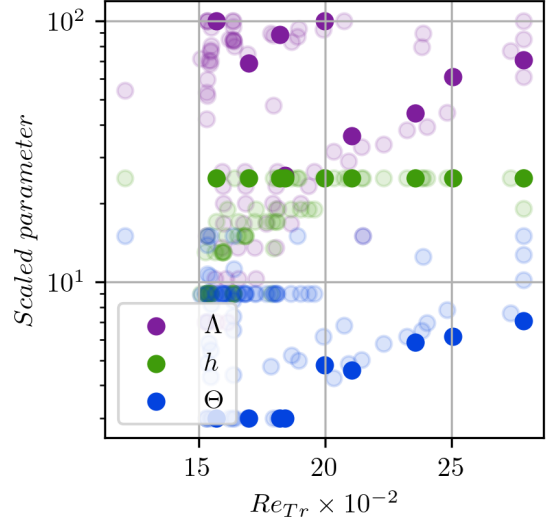
(b) The three varied parameters during the optimisation scaled to fit in the same figure. The x-axis show the transition Reynolds number. Full markers indicate Pareto-optimal points, while opaque ones represent suboptimal configurations.

Figure 2. Results of the three-variable optimisation.

Table 3. Results of the three-variable optimisation

Name	$\hat{\Lambda}$ (mm)	$\hat{d}/\hat{\Lambda}$ (−)	$\hat{\Theta}$ (°)	$\hat{h}$ (mm)	Re_{Tr} (−)	$e_{\max}^N$ (−)
Sz2024	26.5	0.5	9	1.9	1950	1.71
S2015	13	0.25	9	1.3	1793	3.93
Opt1	76.9	0.5	7.58	2.5	> 2781*	1.91
Opt2	61.1	0.5	6.15	2.5	2503	0.62

*There was no transition detected within the computational domain.

The well-known phenomena of the transitional phase overshooting the turbulent phase was neglected.

Due to this effect the results can vary based on the length of the integration, thus the calculation was executed for multiple streamwise coordinates shown with grey dashed lines. In dimensional form, these are the following: $x|_{Re_\delta=1500} = 5.5(m)$, $x|_{Re_\delta=2000} = 9.8(m)$, $x|_{Re_\delta=2500} = 15(m)$, $x|_{Re_\delta=2781} = 19(m)$. The results can be seen in Table 4. In addition, the values for natural transition of the Blasius boundary layer are also included in Table 4.

This shows that, given a shorter body ($L = 5.5(m)$), the drag coefficient between that of a flat plate and of a flow modulated by MVGs can increase by as much as 78%. On the other hand, the strategy works well on longer bodies ($L = 19(m)$), where the same metric can be decreased by 89%. The explanation for this large difference is twofold. In the laminar regime, the vortices generated by the MVGs increase the friction losses. However, by remaining laminar for a much longer distance, the difference in friction between the laminar and turbulent regimes compensates for the higher initial loss.

4. SUMMARY

This paper presents an optimisation method for the geometric properties MVGs, based on local linear stability analysis. Building on prior studies, the base flow near the MVG was computed using 3D CFD simulations, while the downstream evolution of the streaky boundary layer was predicted using the BRE. The stability analysis was performed by solving the BiGlobal stability equations, conducting two sets of calculations for each MVG configuration: one for the modified TS waves and another for identifying potential secondary instabilities that could promote transition. Transition location was estimated using the e^N method for the TS waves with a conservative $N = 7$ value, while for secondary instabilities, the maximum N factor was computed as a destabilisation indicator in the absence of a specific N value. These criteria were used as objectives in a multi-objective Bayesian optimisation approach to find new MVG configurations, which, based on our criteria, outperform previously investigated MVGs. The findings of this study should be further examined through experimental validation or high-fidelity direct numerical simulations.

Table 4. Drag results

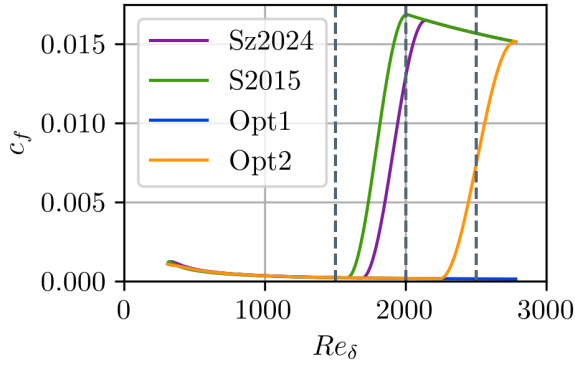| Name	$c_D\|_{Re_\delta=1500}$	$c_D\|_{Re_\delta=2000}$	$c_D\|_{Re_\delta=2500}$	$c_D\|_{Re_\delta=2781}$
Blasius	$2.15 \cdot 10^{-4}$	$8.18 \cdot 10^{-4}$	$15.91 \cdot 10^{-4}$	$20.80 \cdot 10^{-4}$
S2015	$3.66 \cdot 10^{-4}$	$7.44 \cdot 10^{-4}$	$14.43 \cdot 10^{-4}$	$16.57 \cdot 10^{-4}$
Sz2024	$3.90 \cdot 10^{-4}$	$5.19 \cdot 10^{-4}$	$12.46 \cdot 10^{-4}$	$14.98 \cdot 10^{-4}$
Opt1	$3.83 \cdot 10^{-4}$	$3.01 \cdot 10^{-4}$	$2.50 \cdot 10^{-4}$	$2.29 \cdot 10^{-4}$
Opt2	$3.82 \cdot 10^{-4}$	$2.99 \cdot 10^{-4}$	$2.71 \cdot 10^{-4}$	$5.56 \cdot 10^{-4}$

Figure 3. The skin friction coefficients for different configurations. The x-axis shows the non-dimensional streamwise coordinate, Re_δ and the y-axis shows the local friction coefficient c_f. Note that the Opt1 configuration stayed laminar throughout the computational domain ($x1 = 19(m)$).

ACKNOWLEDGEMENTS

REFERENCES

[1] Siconolfi, L., Camarri, S., and Fransson, J. H. M., 2015, "Stability analysis of boundary layers controlled by miniature vortex generators", *Journal of Fluid Mechanics*, Vol. 784, pp. 596–618.

[2] Sattarzadeh, S. S., and Fransson, J. H. M., 2014, "Experimental investigation on the steady and unsteady disturbances in a flat plate boundary layer", *Physics of Fluids*, Vol. 26, p. 124103.

[3] Szabó, A., Nagy, P. T., De Baets, G., Vanierschot, M., and Paál, G., 2024, "Stability analysis of a streaky boundary layer generated by miniature vortex generators", *Computers and Fluids*, Vol. 269, p. 106123.

[4] Sattarzadeh, S. S., and Fransson, J. H. M., 2015, "On the scaling of streamwise streaks and their efficiency to attenuate Tollmien-Schlichting waves", *Experiments in Fluids*, Vol. 56, p. 58.

[5] Ament, S., Daulton, S., Eriksson, D., Balandat, M., and Bakshy, E., 2025, "Unexpected Improvements to Expected Improvement for Bayesian Optimization", `2310.20708`.

[6] Kachanov, Y. S., 1994, "Physical Mechanisms of Laminar-Boundary-Layer Transition", *Annual Review of Fluid Mechanics*, Vol. 26, pp. 411–482.

[7] Herbert, T., 1988, "Secondary Instability of Boundary Layers", *Annual Review of Fluid Mechanics*, Vol. 20, pp. 487–526.

[8] Gad-el-Hak, M., 2000, *Flow Control: Passive, Active, and Reactive Flow Management*, Cambridge University Press, ISBN 9780521770064.

[9] Xu, H., Lombard, J. E. W., and Sherwin, S. J., 2017, "Influence of localised smooth steps on the instability of a boundary layer", *Journal of Fluid Mechanics*, Vol. 817, pp. 138–170.

[10] Luchini, P., and Trombetta, G., 1995, "Effects of riblets upon flow stability", *Applied Scientific Research*, Vol. 54, pp. 313–321.

[11] Nagy, P. T., Szabó, A., and Paál, G., 2022, "The effect of spanwise and streamwise elastic coating on boundary layer transition", *Journal of Fluids and Structures*, Vol. 110 (103521).

[12] Cossu, C., and Brandt, L., 2004, "On Tollmien-Schlichting-like waves in streaky boundary layers", *European Journal of Mechanics - B/Fluids*, Vol. 23, pp. 815–833.

[13] Fransson, J. H. M., Talamelli, A., Brandt, L., and Cossu, C., 2006, "Delaying Transition to Turbulence by a Passive Mechanism", *Physical Review Letters*, Vol. 96, p. 064501.

[14] Fransson, J. H., 2015, "Transition to Turbulence Delay Using a Passive Flow Control Strategy", *Procedia IUTAM*, Vol. 14, pp. 385–393, iUTAM_ABCM Symposium on Laminar Turbulent Transition.

[15] Pearce, H. H., 1961, "Shock-induced separation and its prevention by design and boundary layer control", G. V. Lachmann (ed.), *Boundary layer and flow control: its principles and application*, Vol. 2, Pergamon Press, pp. 1166–1344.

[16] Andersson, P., Brandt, L., Bottaro, A., and Henningson, D., 2001, "On the breakdown of boundary layer streaks", *Journal of Fluid Mechanics*, Vol. 428, pp. 29–60.

[17] Shahinfar, S., Sattarzadeh, S. S., Fransson, J. H. M., and Talamelli, A., 2012, "Revival of Classical Vortex Generators Now for Transition Delay", *Phys Rev Lett*, Vol. 109, p. 74501.

[18] Fransson, J. H. M., and Talamelli, A., 2012, "On the generation of steady streamwise streaks in flat-plate boundary layers", *Journal of Fluid Mechanics*, Vol. 698, pp. 211–234.

[19] Shahinfar, S., Fransson, J. H. M., Sattarzadeh, S. S., and Talamelli, A., 2013, "Scaling of streamwise boundary layer streaks and their ability to reduce skin-friction drag", *Journal of Fluid Mechanics*, Vol. 733, pp. 1–32.

[20] Sattarzadeh, S. S., Fransson, J. H. M., Talamelli, A., and Fallenius, B. E. G., 2014, "Consecutive turbulence transition delay with reinforced passive control", *Physical Review E*, Vol. 89, p. 061001.

[21] Downs, R. S., Fallenius, B. E. G., Fransson, J. H. M., and Mårtensson, H., 2017, "Miniature Vortex Generators for Flow Control in Falkner–Skan Boundary Layers", *AIAA Journal*, Vol. 55, pp. 352–364.

[22] Shahinfar, S., Sattarzadeh, S. S., and Fransson, J. H. M., 2014, "Passive boundary layer control of oblique disturbances by finite-amplitude streaks", *Journal of Fluid Mechanics*, Vol. 749, pp. 1–36.

[23] Weingärtner, A., Mamidala, S. B., and Fransson, J. H., 2023, "Application of Miniature Vortex Generators for Boundary Layer Transition Delay", *AIAA Paper 2023-0097*.

[24] Nobis, H., Schlatter, P., Wadbro, E., Berggren, M., and Henningson, D., 2023, "Topology optimization of roughness elements to delay modal transition in boundary layers", F. Auteri, D. Fabre, F. Giannetti, and A. Hanifi (eds.), *Progress in Flow Instability, Transition and Control*, ERCOFTAC, 15TH ERCOFTAC SIG33 WORKSHOP, p. 44.

[25] Bagheri, S., and Hanifi, A., 2007, "The stabilizing effect of streaks on Tollmien-Schlichting and oblique waves: A parametric study", *Physics of Fluids*, Vol. 19, p. 78103.

[26] Garnett, R., 2023, *Bayesian Optimization*, Cambridge University Press.

[27] Diessner, M., O'Connor, J., Wynn, A., Laizet, S., Guan, Y., Wilson, K., and Whalley, R. D., 2022, "Investigating Bayesian optimization for expensive-to-evaluate black box functions: Application in fluid dynamics", *Frontiers in Applied Mathematics and Statistics*, Vol. 8.

[28] Pederson, C. C., Choudhari, M. M., Zhou, B. Y., Paredes, P., and Diskin, B., 2020, "Shape optimization of vortex generators to control mack mode amplification", *AIAA AVIATION 2020 FORUM*, Vol. 1 PartF.

[29] Klauss, C. W., Pederson, C. C., Paredes, P., Choudhari, M. M., and Diskin, B., 2022, "Stability Analysis of Streaks Induced by Optimized Vortex Generators", *AIAA Paper 2022-3249*.

[30] Schrauf, G., 2004, "Large-Scale Laminar Flow Tests Evaluated with Linear Stability Theory", *Journal of Aircraft*, Vol. 41 (2), pp. 224–230.

[31] Schrauf, G. H., and von Geyr, H., 2020, *Simplified Hybrid Laminar Flow Control for the A320 Fin - Aerodynamic and System Design, First Results*.

[32] Schrauf, G. H., and von Geyr, H., 2021, *Simplified Hybrid Laminar Flow Control for the A320 Fin. Part 2: Evaluation with the e^N-method*.

[33] Theofilis, V., 2003, "Advances in global linear instability analysis of nonparallel and three-dimensional flows", *Progress in Aerospace Sciences*, Vol. 39 (4), pp. 249–315.

[34] ANSYS Inc., 2021, *ANSYS 21 R2 CFX Theory Guide*.

[35] Geuzaine, C., and Remacle, J.-F., 2009, "Gmsh: A 3-D finite element mesh generator with built-in pre- and post-processing facilities", *International Journal for Numerical Methods in Engineering*, Vol. 79 (11), pp. 1309–1331.

[36] Hecht, F., 2012, "New development in freefem++", *Journal of Numerical Mathematics*, Vol. 20 (3-4), pp. 251–266.

[37] Hecht, F., 1998, *BAMG: Bidimensional anisotropic mesh generator*, INRIA.

[38] Balay, S., Gropp, W. D., McInnes, L. C., and Smith, B. F., 1997, "Efficient Management of Parallelism in Object Oriented Numerical Software Libraries", E. Arge, A. M. Bruaset, and H. P. Langtangen (eds.), *Modern Software Tools in Scientific Computing*, Birkhäuser Press, Boston, MA, pp. 163–202.

[39] Roman, J. E., Campos, C., Dalcin, L., Romero, E., and Tomas, A., 2022, "SLEPc Users Manual", *Tech. Rep. DSIC-II/24/02 - Revision 3.18*, D. Sistemes Informàtics i Computació, Universitat Politècnica de València.

[40] Amestoy, P. R., Buttari, A., L'Excellent, J.-Y., and Mary, T., 2019, "Performance and Scalability of the Block Low-Rank Multifrontal Factorization on Multicore Architectures", *ACM Trans Math Softw*, Vol. 45 (1).

[41] Balandat, M., Karrer, B., Jiang, D. R., Daulton, S., Letham, B., Wilson, A. G., and Bakshy, E., 2020, "BoTorch: A Framework for Efficient Monte-Carlo Bayesian Optimization", *Advances in Neural Information Processing Systems 33*.

[42] Schultz-Grunow, F., 1941, "New Frictional Resistance Law for Smooth Plates", .